RSC Advances

PAPER

View Article Online
View Journal | View Issue

Cite this: *RSC Adv.*, 2025, **15**, 50337

Insights into electric- and thermal-induced decomposition and gas evolution of silicone rubber through experiments and molecular simulations

Jingwen Gong,[a] Qi Zhao,[b] Jingtao Huang,*[ac] Zhuocheng Ye,[a] Zihao Wang,[a] Yidong Chen[a] and Wei Gong*[a]

This study investigates the degradation state of silicone rubber (SiR) under electric and thermal fields by analyzing its gas-evolution characteristics. The goal is to provide a new diagnostic approach for high-voltage cable accessories. Thermogravimetry-infrared spectroscopy (TG-IR) was used to trace the thermal decomposition products. Electrical breakdown was simulated through discharge experiments. Density functional theory (DFT) calculations and reactive force field (ReaxFF) molecular dynamics simulations were employed to verify the reaction mechanisms and decomposition pathways. The results show that under electric field, SiR mainly produces CH_4, C_2H_2, and silane (SiH_4), accompanied by CO and CO_2. Under thermal field, the main products are CH_2O, CH_4, hexamethylcyclotrisiloxane (D3), and octamethylcyclotetrasiloxane (D4), along with oxidative gases such as CO_2. Molecular simulations revealed differences in microscopic decomposition pathways. A normalized infrared spectral database was also established based on DFT calculations. Overall, this work links macroscopic gas-evolution behavior with microscopic mechanisms and diagnostic applications. It systematically elucidates the decomposition behavior of SiR under electric and thermal fields and provides a theoretical foundation for gas-infrared-based fault diagnosis in cable accessories.

Received 29th September 2025
Accepted 27th November 2025

DOI: 10.1039/d5ra07405c

rsc.li/rsc-advances

1 Introduction

With the rapid growth of urbanization and electricity demand, power transmission cables have become critical infrastructure for ensuring the stable operation of power systems and supporting economic development. High-voltage cables are widely used in urban power grids, and their safety and reliability directly affect power supply quality and societal efficiency.[1] Among the components of cable systems, accessories are considered as the weakest link. They are more prone to insulation performance degradation during long-term service, which may threaten the stability of the entire network. Silicone rubber (SiR), owing to its excellent electrical insulation, thermal stability, and mechanical flexibility,[2,3] has been extensively used in high-voltage cable accessories.[4] However, under prolonged electric and thermal fields, SiR gradually undergoes aging and releases characteristic gaseous products.[5]

To investigate this phenomenon, previous studies have used thermogravimetric analysis (TGA),[6] Fourier transform infrared spectroscopy (FTIR), gas chromatography-mass spectrometry (GC-MS), and scanning electron microscopy (SEM) to analyze the gas-evolution behavior of SiR under electric and thermal fields.[7,8] Most of these studies have focused on the analysis of gas evolution during thermal decomposition. In contrast, investigations on gas generation under electric field remain scarce. Comparative studies of electrical breakdown-induced decomposition *versus* thermal decomposition are particularly rare, and the differences in gas evolution under these conditions have not been fully explored. Although typical gaseous products such as CH_2O and cyclic siloxanes generated during thermal decomposition have been identified,[9,10] the intrinsic relationship between molecular chain scission pathways and gas formation remains unclear. Consequently, current diagnostic techniques are still limited in their ability to elucidate the underlying mechanisms of SiR decomposition.

Previous studies have shown that the decomposition behavior of SiR is strongly influenced by both electric and thermal field conditions. In most reports, the thermal decomposition process is divided into three temperature stages. The low-temperature stage occurs below 350 °C and is characterized by surface moisture evaporation. The medium-temperature stage, between 350 °C and 450 °C, involves side-chain scission. The high-temperature stage, above 450 °C, is where the maximum weight loss occurs. This is due to extensive bond cleavage and recombination.[11] However, this coarse

[a]*College of Electrical Engineering, Sichuan University, Chengdu, 610065, Sichuan, China. E-mail: Gwei349@163.com*
[b]*State Grid Sichuan Electric Power Company Leshan Power Supply Company, 614000, China*
[c]*College of Electrical Engineering, Northwest Minzu University, Lanzhou, 730030, China*

classification does not fully capture the complexity of SiR decomposition under real service conditions. Moreover, most existing studies have been limited to single thermal effects, and systematic investigations of decomposition mechanisms under coupled electro-thermal fields remain scarce.

ReaxFF molecular dynamics simulations have shown that high-temperature thermal degradation of SiR mainly generates CH_4, small-ring cyclosiloxanes, and methyl radicals as gaseous products.[12–17] However, these simulation results differ significantly from those obtained by dissolved gas analysis (DGA). DGA primarily detects gases dissolved in liquid insulating oils,[18] whereas SiR is a solid material whose decomposition products are mainly solid SiO_2.[19] The characteristic gases detected by the two methods also differ considerably.

In addition, some studies on other polymer systems have used the electron force field (EFF) to model discharge-induced decomposition.[20] The method is accurate at the microscopic level, but it is computationally expensive. It scales poorly for large polymer systems and is difficult to extend to engineering applications. To address this limitation, researchers have introduced charge transfer with polarization current equalization (QTPIE). QTPIE represents intramolecular charge distribution and equilibration under external electric fields more accurately. It provides a new route to probe decomposition mechanisms of polymers under complex electro-thermal conditions and helps overcome the limitations of conventional methods in large-scale simulations.

Accordingly, this work combines experiments with molecular simulations to investigate the gas-evolution behavior of SiR under various electric and thermal field conditions. A normalized infrared spectral database of characteristic gases is established. And reveal the generation rules of gas products under different environmental conditions.

2 Materials and methods

2.1 Sample preparation and instrumentation

The experimental material was obtained from 110 kV SiR cable joints, in which the SiR formulation contains approximately 15% inorganic filler (SiO_2).[21,22] The samples were prepared by slicing the joints with a cutting machine, ensuring that their composition is consistent with that used in engineering applications.

The instruments used in this study were as follows: Fourier transform infrared spectrometer (FTIR, Nicolet 6700, Thermo Fisher Scientific, USA); thermogravimetric analyzer (TGA, Pyris, PerkinElmer, USA); and gas chromatograph (GC, GC112N, Shanghai Analytical Instrument Co., China).

2.2 Electrical gas evolution experiments of SiR

The breakdown decomposition setup for SiR in air is shown in Fig. 1. The electrode plates were sandwiched between two SiR sheets and the assembly was placed in a sealed gas-generation chamber. The discharge strength was controlled by adjusting the electrode gap to 1, 3, and 5 mm. The applied voltage was then increased stepwise at a rate of 1 kV min^{-1} until a high-energy discharge occurred and caused breakdown of the material. For electrode gaps of 1, 3, and 5 mm, the breakdown voltages in air were approximately 1.4, 2.0, and 4.8 kV, respectively, while those in argon atmosphere were 1.3, 2.8, and 4.7 kV. The discharge energy was calculated using the capacitor energy relation $E = 0.5CV_{bd}^2$ with $C = 10$ pF.[23] For electrode gaps of 1, 3, and 5 mm, the discharge energies in air atmosphere were 9.8, 20, and 115.2 μJ, respectively, and those in argon atmosphere were 8.45, 39.2, and 110.45 μJ. The gaseous products were collected using a syringe and analyzed offline by FTIR to obtain the infrared spectra of the decomposition products.

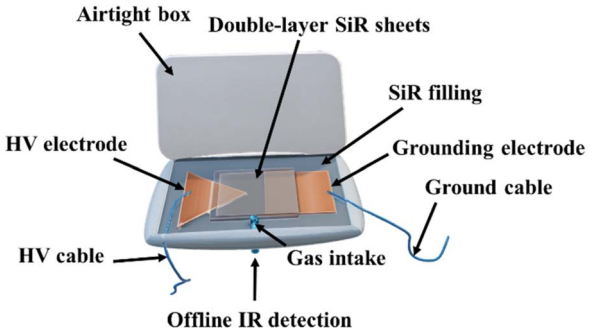

Fig. 1 Experimental setup diagram for breakdown gas production process.

2.3 Thermal gas evolution experiments of SiR

Thermal degradation characteristics were analyzed using TG-IR and GC experiments. These two methods cover different gas species. TG-IR provided thermal decomposition curves and infrared spectra of polar gases but could not detect H_2. GC analysis successfully quantified the concentrations of seven gases: H_2, CO, CO_2, C_2H_4, C_2H_2, CH_4, and C_2H_6. However, it did not detect any other gaseous products.

In the TG-IR experiments, the sample temperature was increased under programmed control using the thermogravimetric analyzer. Volatile products released during decomposition were continuously monitored by the FTIR spectrometer. The tests were conducted in air and argon atmosphere, with the temperature range set from 50 °C to 800 °C and a heating rate of 50 °C min^{-1}. GC experiments were carried out by placing 0.1 g of SiR in a gas washing bottle, with the temperature precisely controlled by an electric heater. After gas generation, the gaseous products were qualitatively and quantitatively analyzed using a gas chromatograph equipped with a molecular sieve column and an alumina column, with detection performed by FID and TCD, respectively. In the muffle furnace experiments, when the temperature exceeded 400 °C, 0.02 g of SiR was loaded into an alumina threaded crucible and heated to produce gases; the released products were collected in a sealed plastic bag equipped with a gas valve and subsequently analyzed by GC under the same conditions. Prior to quantitative measurements, a seven-component mixed standard gas was used for calibration to ensure the accuracy of concentration determination. All GC-derived gas concentrations were normalized to the sample

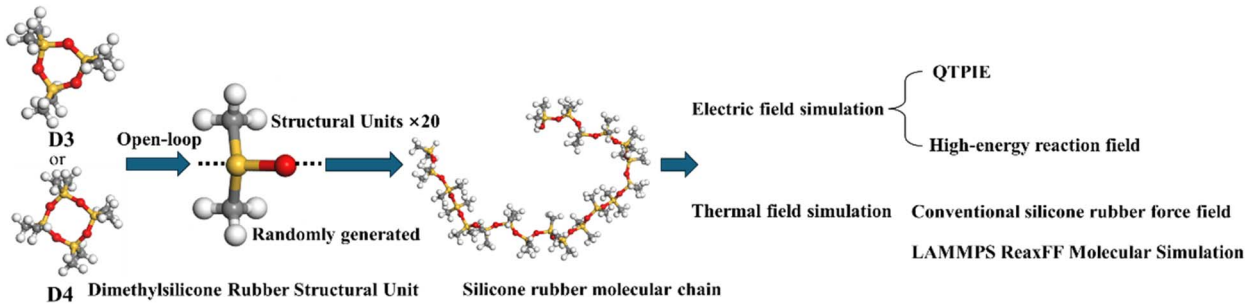

Fig. 2 Construction and simulation procedure of silicone rubber molecular models.

mass by dividing the measured concentration of each component by the corresponding sample amount, and the results were finally expressed as gas concentration per gram of sample.

2.4 MD simulations and DFT calculations of SiR decomposition

To accurately simulate the decomposition behavior of SiR under electric and thermal fields, two types of polydimethylsiloxane (PDMS) models were first constructed using Packmol: a single-chain model and a folded-chain model. The folded-chain model contained five PDMS single chains, and the folded conformations were randomly generated using the Monte Carlo method. Energy minimization and relaxation were then performed in LAMMPS under the ReaxFF reactive force field to eliminate unreasonable stresses and conformations. Decomposition simulations were carried out in air and argon atmospheres. In air atmosphere, 40 O_2 molecules were added to the simulation box, whereas in argon atmosphere the system contained only the pure polymer (Fig. 2).

In the thermal decomposition simulations, the system was gradually heated to 1500 K under a constant-volume, constant-temperature (*NVT*) ensemble, where 1500 K was adopted as an "accelerated condition" rather than the actual decomposition temperature to speed up the decomposition process.[24] Temperature control was achieved using a Berendsen thermostat with a damping constant of 25 fs to promote chain scission and structural rearrangement. For the electric field simulations, the QTPIE method was used to achieve dynamic charge equilibration. An external electric field of 3 kV mm^{-1} was applied to the two ends of the simulation box to enhance molecular polarization and facilitate chain breakage. Both the single-chain and folded-chain models were simulated. The single-chain model was used to analyze the microscopic mechanisms of small-molecule generation, whereas the folded-chain model, being closer to real systems, allowed statistical analysis of the yields of characteristic gaseous products. The molecular structural evolution during decomposition was visualized using Open Visualization Tool (OVITO), and the formation trends of key products were quantified.

The gas release during SiR decomposition was obtained from the molecular dynamics (MD) simulations. Vibrational analyses based on density functional theory (DFT) were then performed. These analyses calculated the vibrational modes and infrared absorption frequencies of the characteristic gases. These calculations were carried out in Gaussian at the B3LYP/def2-SVP level of theory.[25] Because the harmonic approximation and the solution of the Schrödinger equation introduce systematic errors,[26] the predicted IR frequencies are typically higher than the experimental fundamentals. Following the literature,[27,28] a scaling factor of 0.9671 was applied to correct the calculated frequencies. The spectra were then Gaussian-broadened using the Multiwfn program to achieve better agreement with the experimental data.

3 Results and discussion

3.1 Analysis of gas evolution from electrical breakdown of SiR

Gas identification in FTIR spectroscopy relies on the characteristic vibrational absorption peaks of molecules, enabling rapid recognition of multiple gas components. Because gas molecules contain few atoms, their characteristic bands are concentrated in specific wavenumber ranges, which enables rapid identification of multiple components in a complex gas mixture. However, FTIR is insensitive to non-polar molecules such as H_2 and therefore cannot detect their presence. Based on FTIR analysis, the gas products from SiR decomposition under electrical breakdown were systematically investigated. Shown in Fig. 3, the main products generated after breakdown were CH_4, H_2O, C_2H_2, CO_2, and CO. By comparing the spectra under different atmospheres, it can be seen that the characteristic peaks of Si–H and C_2H_2 are more pronounced in argon atmosphere, although the overall differences remain limited. This is mainly because the presence of oxygen promotes the cleavage or transformation of C≡C bonds, thereby reducing the yield of C_2H_2.

Moreover, H_2 radicals generated during discharge can react with silicon atoms to form Si–H-containing species, such as silane (SiH_4). Although cyclic siloxanes are important monomeric units of SiR, their yields were low under breakdown conditions because the reaction was extremely rapid and chain rearrangement was limited. As a result, their FTIR characteristic bands were weak (Fig. 3).

3.2 Analysis of gas evolution from thermal decomposition of SiR

As shown in Fig. 4, thermogravimetric analysis reveals four characteristic temperatures for SiR at 370, 615, 665, and 754 °C.

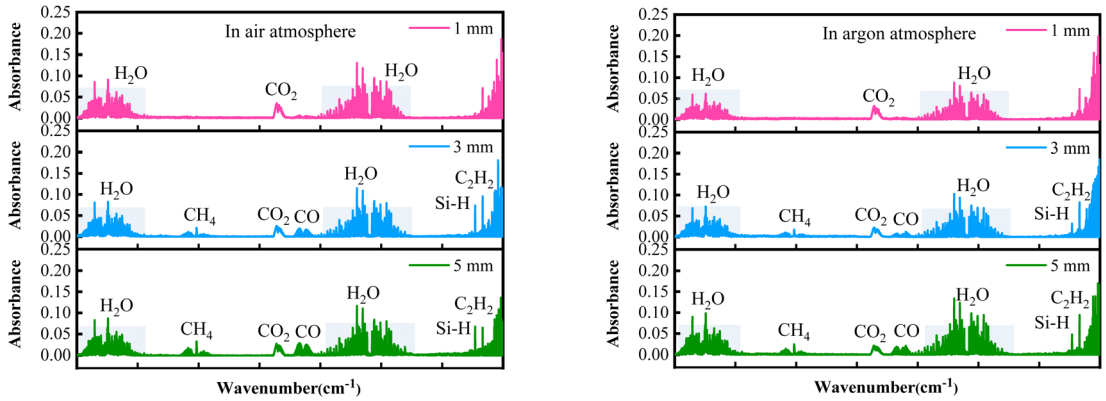

Fig. 3 Infrared spectra of SiR gas production in (a) air and (b) argon atmospheres.

At high temperatures, the residual mass remains at approximately 60%, which is mainly composed of the original inorganic filler SiO_2 and SiO_2 formed from the thermal degradation of SiR at elevated temperatures.[29] Because these temperatures showed a relatively rich composition and noticeable release of characteristic gases, they were selected for detailed analysis. The first corresponds to the onset of decomposition at 370 °C, followed by two decomposition-rate maxima at 615 °C and 754 °C, and a transition temperature at 665 °C. This selection allowed the relationship between characteristic gaseous species and different decomposition stages to be established.

To more intuitively illustrate the effects of atmosphere and temperature on the gas-evolution behavior, three-dimensional FTIR spectra (Fig. 5) and GC chromatograms (Fig. 6) were acquired under both air and argon atmospheres, and several representative temperatures were selected for analysis in conjunction with the TG curves. The results show that, below the onset decomposition temperature in argon atmosphere, only H_2O and trace amounts of CO_2 are detected, indicating that the material structure remains largely unchanged. At the decomposition temperature, small amounts of CH_4 and CO_2 appear in the products. As the temperature increases above the decomposition threshold, the signals associated with Si-containing groups (*e.g.*, Si–CH_3, Si–O–Si, Si–$(CH_3)_2$) become more pronounced,[30–33] suggesting that the cleavage and rearrangement of the structural units in SiR are significantly intensified at elevated temperatures. Previous studies have shown that, at high temperatures, these structural units can undergo scission and cyclization to form low-molecular-weight cyclic siloxanes such as hexamethylcyclotrisiloxane (D3) and octamethylcyclotetrasiloxane (D4).[34–39]

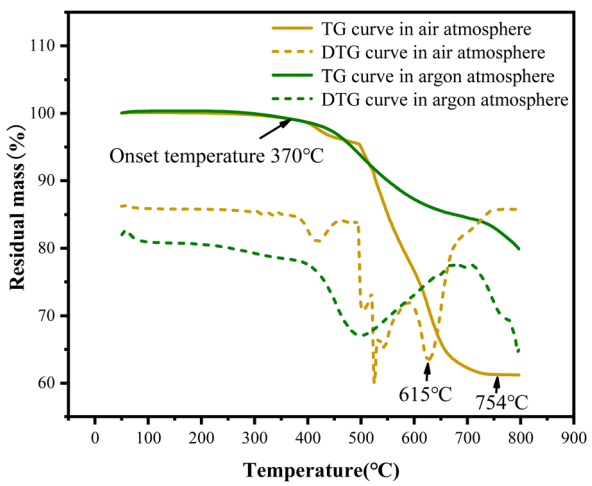

Fig. 4 SiR decomposition thermogravimetric analysis.

3.3 ReaxFF-based MD simulations of gas evolution from SiR decomposition

Experimental observation of radical reaction pathways during SiR decomposition is difficult. Additionally, distinguishing the characteristic peaks of similar gases in mixed-gas FTIR spectra is challenging. To address these issues, this study employed ReaxFF-based reactive molecular dynamics simulations. These simulations were used to characterize gas-generation behavior under various factors at the atomic scale. Thermal decomposition was simulated by setting the system temperature to the target decomposition level. Electrical breakdown was modeled by applying an external electric field and using a reactive force field that accounts for interatomic interactions, while raising the system temperature to mimic the transient high-temperature conditions during discharge.

3.3.1 Reactive MD simulations of gas evolution. Reactive MD simulations using ReaxFF were performed to analyze the decomposition mechanism of SiR at the atomic scale under electrical breakdown conditions. As shown in Fig. 7(a), the siloxane backbone was the primary site of bond cleavage. In the early stage (25 ps), –CH_3 groups detached from the chains, generating free radicals. As the reaction proceeded, by 325 ps the Si–O–Si skeleton gradually degraded, oxygen-containing groups detached, and free methyl radicals recombined to form CH_4 and C_2H_2. This indicates partial reconstruction of the carbon chains and agrees well with the experimentally observed increases in CH_4 and C_2H_2. In the later stage (5625 ps), the carbon chains underwent deep scission and became more unsaturated, leading to further increases in CH_4 and C_2H_2 yields. Simultaneously, Si–H-containing species such as SiH_4

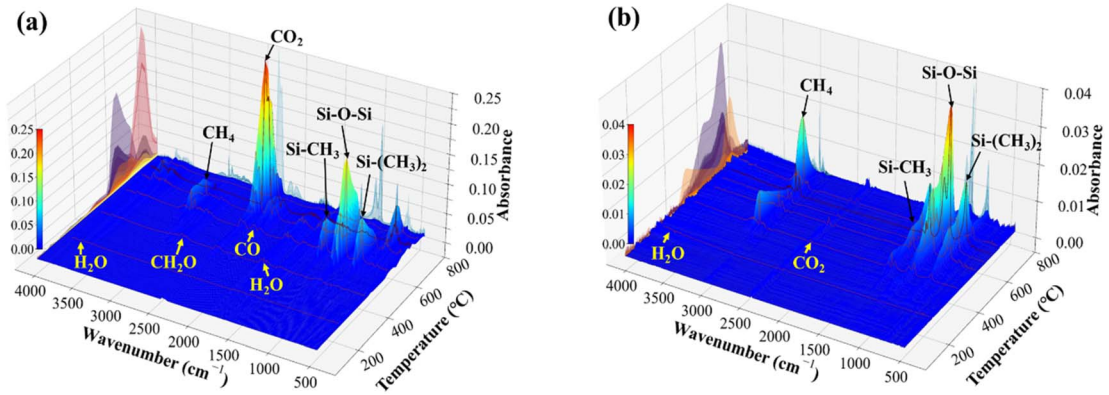

Fig. 5 Three-dimensional IR spectra of the gas release during thermal decomposition of SiR in (a) air and (b) argon atmospheres.

were formed, consistent with the enhanced Si–H peaks observed in the FTIR spectra. By the end of the simulation (25 000 ps), the SiR network was almost completely degraded, resulting in the generation of large quantities of small-molecule gases. The strong agreement between simulation and experimental results further validated the accuracy of the molecular dynamics approach. It should be noted that although 1500 K is much higher than the actual decomposition temperature, this condition is mainly employed to accelerate the reaction process and to elucidate the decomposition mechanism and relative trends, rather than to directly extrapolate absolute rates or service lifetimes.[40]

Unlike electrical breakdown, the thermal decomposition of SiR favored high-temperature rearrangement. The ReaxFF-based MD simulations were further used to investigate this process. As shown in Fig. 7(b), at the early stage (25 ps), side chains were cleaved first, producing free radicals that provided the basis for subsequent high-temperature reactions. By 675 ps, the main chain began to disintegrate, and some fragments underwent rearrangement, producing H_2 and CH_4. This observation agrees well with the CH_4 characteristic peaks detected in the FTIR spectra. At 4175 ps, elevated temperature promoted further scission and rearrangement of the siloxane backbone, leading to the formation of cyclic siloxanes such as D4, which are typical products of thermal decomposition, together with a certain amount of CO. By 25 000 ps, the reaction approached completion. The residual structure was dominated by Si–O–Si linkages, with only trace amounts of CH_4 and CO present. This result is consistent with the experimental observation of strong Si–O–Si characteristic peaks and weak small-molecule peaks.

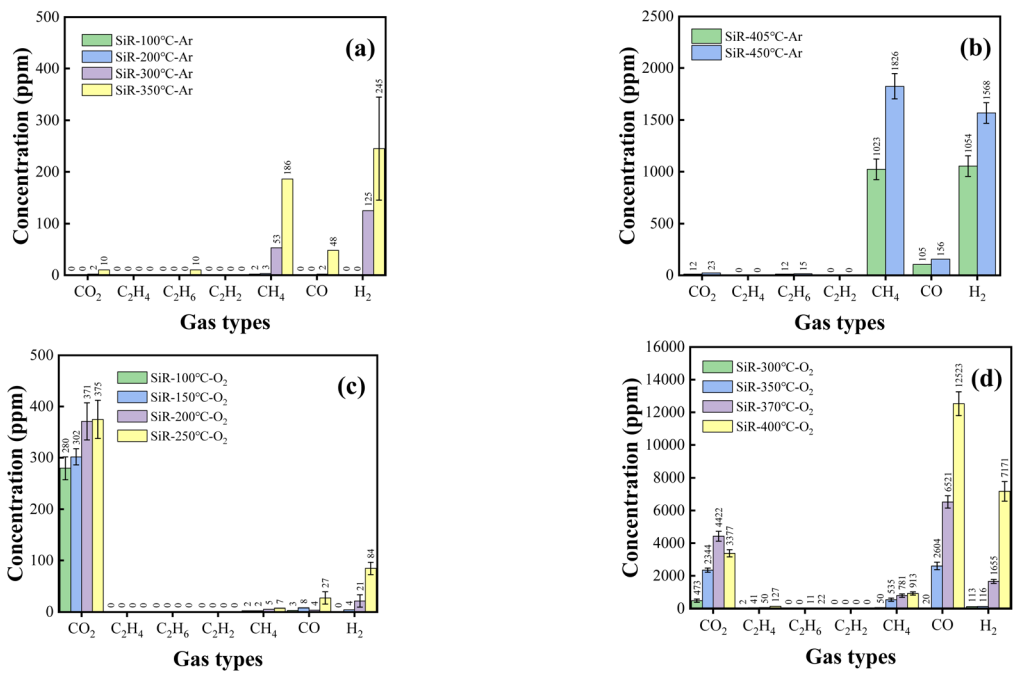

Fig. 6 Gas chromatography results of SiR gas production at different temperatures in (a) argon 100–350 °C, (b) argon 405–450 °C, (c) oxygen 100–250 °C, and (d) oxygen 300–400 °C atmospheres.

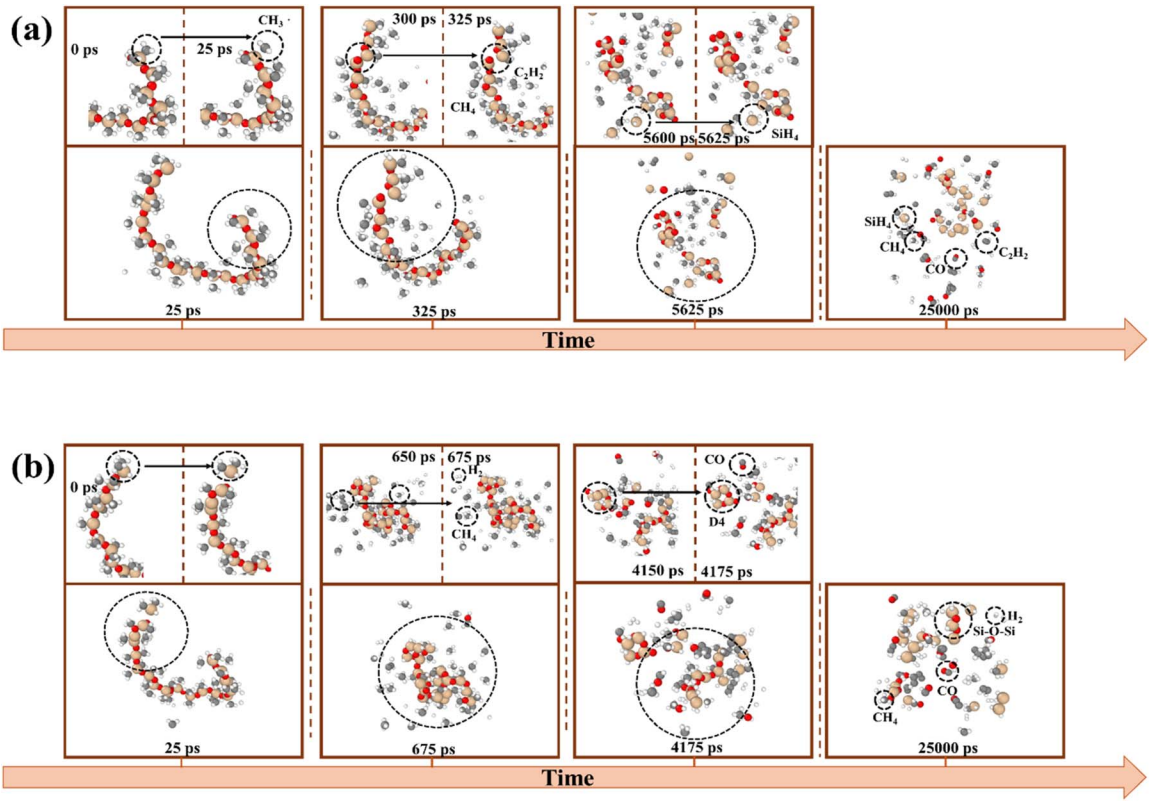

Fig. 7 Snapshots of gas formed during simulation for SiR, (a) under electric field condition; (b) under thermal condition.

3.3.2 DFT-based construction of an infrared spectral database for characteristic gases. To further analyze and identify the gaseous products generated during SiR decomposition, an infrared spectral database of characteristic gases was established using DFT calculations. The database was constructed from the vibrational spectra of individual molecules. This allows the peak intensities to be normalized to a reference concentration, enabling quantitative comparison across different species. In addition, some characteristic gases may exist in liquid or even solid form at room temperature, similar to substances such as alcohols that are only partially volatile. By establishing the infrared spectral library through DFT calculations, hazardous gas-phase experiments—where the gases may be toxic or flammable—can be avoided, while still providing a reliable reference for spectral analysis. Representative IR spectra of selected gases are shown in Fig. 8. Characteristic hydrocarbon peaks appear near 3000 cm^{-1}, including those of CH_4 and CH_2O. The region near 1000 cm^{-1} corresponds primarily to Si–H and Si–O vibrations, including cyclic siloxanes such as D3 and D4 as well as SiH_4. The resulting spectral database covers the major small-molecule and Si-containing species relevant to failure diagnosis and thermal decomposition of SiR, providing a theoretical foundation for real-time gas detection.

3.3.3 Incremental IR spectral calculations of gas components. The stage-resolved formation characteristics of incremental gases-defined as the gaseous species newly generated at each stage relative to the preceding one-differed markedly in air and in argon, and between thermal and discharge conditions. Statistical analysis of these incremental gases enables the identification of stage-specific gas-evolution features. For thermal decomposition, the stages were first divided according to the characteristic temperatures obtained from the TG curve. Additional subdivision was performed based on the temperature intervals where significant changes in FTIR spectra were observed, and further refined using the product evolution trends obtained from MD simulations. For electrical breakdown, the stages were defined primarily according to discharge intensity and the corresponding product formation revealed by MD simulations. By integrating results obtained in air and in argon for both thermal and discharge scenarios, the

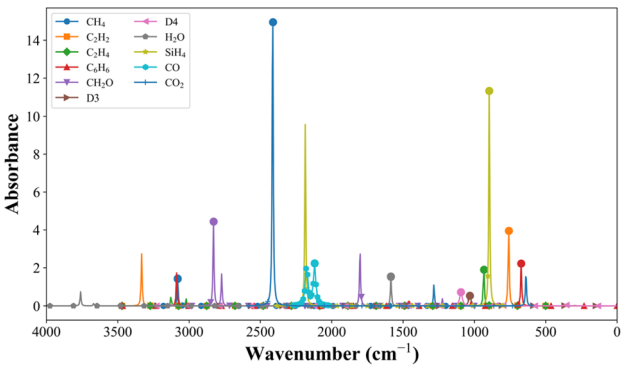

Fig. 8 DFT calculation spectral library.

composition and IR spectral characteristics of the evolved gases were elucidated. These results provide important insights into the stepwise decomposition mechanism of SiR.

3.3.3.1 Incremental gas characteristics under pure thermal conditions. As shown in Fig. 9(a), under purely thermal conditions SiR exhibits almost no pronounced decomposition at the initial stage; only a small fraction of unstable end groups is cleaved, releasing trace amounts of H_2O and CO_2. As the temperature increases, SiR begins to undergo extensive chain scission and releases larger amounts of volatile gaseous products, such as CO and CO_2. In this stage, the siloxane backbone undergoes high-temperature rearrangement to form cyclic siloxanes (D3 and D4), while cleavage of terminal groups generates CH_4. The CH_4 is subsequently oxidized in the presence of oxygen to produce CH_2O. As the temperature further increases and the decomposition approaches completion, the Si–O–Si bonds are almost completely broken, leaving a large amount of solid residue composed mainly of SiO_2 and a partial carbonaceous layer. These carbon-containing particulates and the carbon layer react with oxygen to generate additional CO_2 and CO. Overall, the thermal decomposition of SiR is dominated by end-group scission and backbone rearrangement, which give rise to various small-molecule gaseous products and promote the formation of cyclic siloxanes. At the final stage, the siloxane bonds are completely cleaved, and predominantly solid SiO_2 and a residual carbon layer remain.

3.3.3.2 Incremental gas characteristics under combined thermal and electric fields. High-energy discharge markedly alters the degradation pathways of SiR, as shown in Fig. 9(b). At the initial stage, the main gaseous products are CO and C_2H_2, accompanied by detectable amounts of CO_2 and H_2O.

Under the action of the electric field, the SiR molecular chains undergo pronounced scission, and methyl side groups are detached from the backbone to form radicals, which subsequently recombine to yield small molecules such as CH_4 and C_2H_2. With increasing discharge intensity, chain scission becomes more severe, and hydrogen radicals generated during the discharge react with silicon to form Si–H-containing species, such as SiH_4.

In an oxygen-containing atmosphere, the synergistic effect of discharge and oxygen further enhances chain scission and radical generation, thereby promoting the formation of CH_4 and Si–H-containing compounds. Meanwhile, the participation of oxygen facilitates the cleavage or transformation of C≡C bonds, leading to a decreased yield of C_2H_2. In addition, owing to the extremely short duration of breakdown, chain rearrangement is limited, so the conditions for the formation of cyclic siloxanes are not fully met, resulting in a relatively low yield of cyclic siloxanes. Overall, the decomposition of SiR under an electric field is dominated by chain scission and radical formation, which gives rise to multiple small-molecule gaseous products, particularly CH_4 and C_2H_2, whereas the formation of cyclic siloxanes is comparatively suppressed.

3.3.3.3 Comparative summary of results. Overall, gas evolution during thermal decomposition is primarily governed by thermally induced chain scission and rearrangement reactions, with relatively simple influencing factors. This process mainly produces CO_2 and CO, accompanied by the formation of cyclic siloxanes such as D3 and D4. By contrast, gas generation during electrical decomposition is driven by electro-thermal coupling, which gives rise to more complex reaction pathways. Under the action of the electric field, the molecular chains experience more intense scission and generate abundant radicals, leading to the formation of a larger variety of small-molecule gases, such as CH_4 and C_2H_2. In addition, during electrical decomposition in air, the synergistic effect of the electric field and

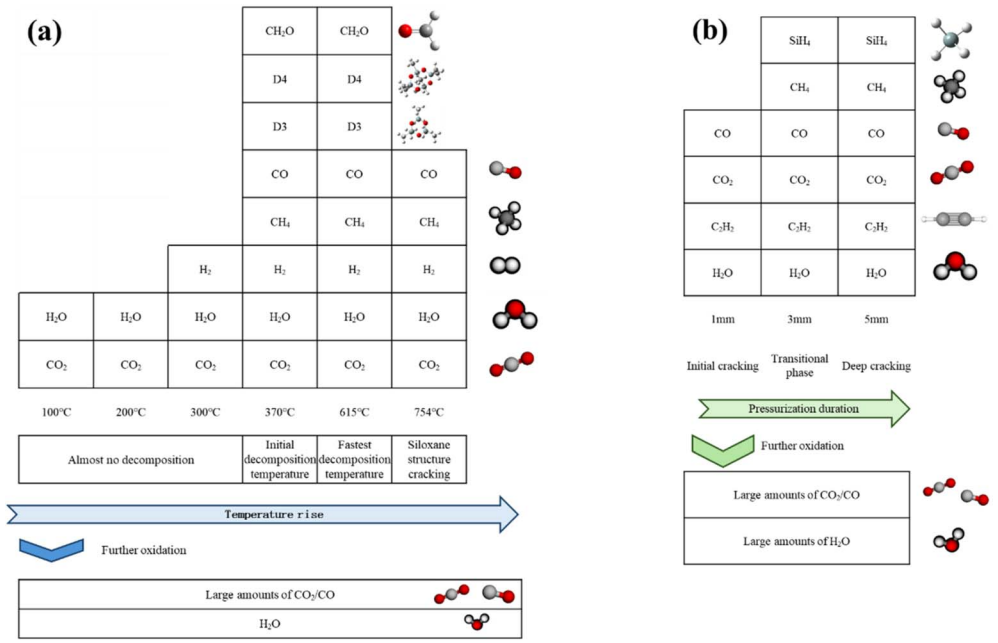

Fig. 9 Decomposition mechanisms of SiR under (a) thermal field and (b) electric field, illustrating incremental gas production under anaerobic and aerobic environments.

Table 1 Comparison of thermal and electrical decomposition of SiR

	Thermal decomposition	Electrical decomposition
Reaction mechanism	Thermally induced chain breakage/rearrangement	Electrothermal coupling chain breakage/free radical generation
Reaction products	CO_2, CO, CH_4, D3, D4	CH_4, C_2H_2, SiH_4
Influencing factors	Temperature	Electric field and temperature

oxygen promotes the cleavage of C≡C bonds and the formation of Si–H compounds. Compared with thermal decomposition, electrical decomposition produces a more diverse range of gaseous species and larger overall amounts of gas. These differences in degradation mechanisms and products highlight the intrinsic distinction between the chemical pathways of electrical and thermal decomposition (Table 1).

4 Conclusions

In this work, the decomposition behavior of SiR under electric field and thermal field was investigated, and its gas generation characteristics were analyzed. By combining experiments with molecular simulations, the mechanisms of gas generation under different conditions were elucidated. The main conclusions are as follows:

(1) Under pure thermal conditions, SiR primarily decomposed to produce CH_2O, CH_4, and Si-containing organics such as D3 and D4, accompanied by a certain amount of oxidative products such as CO_2. Under electric field, the characteristic gases were dominated by C_2H_2, CH_4, and Si-containing compounds such as SiH_4, along with small amounts of CO and other oxidizing molecules. This composition indicates a discharge gas-evolution behavior characterized by low-molecular-weight and highly reactive Si-containing species.

(2) Reactive MD simulations based on ReaxFF revealed the microscopic decomposition mechanisms of SiR under thermal and electric fields. Under thermal conditions, weak bonds such as $-CH_3$ were cleaved first. Free radicals subsequently accumulated and recombined, eventually causing the cleavage of the Si–O–Si backbone and the formation of small cyclic siloxanes. Under electric field, initial scission also occurred at weak bonds. As the applied voltage increased, deeper chain cleavage and unsaturation took place, leading to the generation of CH_4 and SiH_4. However, because the breakdown duration was extremely short, chain rearrangement was insufficient and the yield of cyclic siloxanes was limited. These simulation results were highly consistent with the experimental trends, providing molecular-level insight that is difficult to obtain directly from experiments. Overall, electric field promoted chain scission, whereas thermal field favored structural rearrangement.

(3) The presence of oxygen significantly promoted molecular chain scission and radical reactions, whereas in an inert atmosphere the decomposition proceeded mainly through thermal pyrolysis.

A preliminary FTIR spectral library of characteristic gaseous products from SiR decomposition was established, and an IR-based diagnostic method was proposed. These results provide a technical pathway for gas-phase IR spectroscopy in aging assessment and fault diagnosis of high-voltage cable accessories. This approach is expected to play an important role in early fault warning and diagnosis, thereby reducing the risks of power outages and fire accidents.

Author contributions

J. G. and Q. Z. designed the experiments. J. G. conducted the majority of the experimental work. J. H., Y. C., and Z. Y. performed the gas evolution analysis and conducted the infrared spectroscopy experiments. Z. W. and W. G. were responsible for the molecular dynamics simulations and density functional theory (DFT) calculations. Z. W. and Y. C. assisted in the data analysis and interpretation. J. G., Q. Z., and J. H. wrote the paper.

Conflicts of interest

There are no conflicts to declare.

Data availability

The data that support the findings of this study are available from the corresponding author upon reasonable request.

Supplementary information (SI): detailed information regarding the experimental procedures and analysis results of the study. Specifically, it includes: S1 (details of the electrical decomposition experiments): detailed parameters for the electrical decomposition experiments, including the gas collection setup, step-by-step voltage increase, measured breakdown voltages in air and argon, discharge duration, and an estimation of the discharge energy for various electrode spacings (presented in Table S1 1). S2 (comparison of thermal and electric decomposition mechanisms): a comparative summary (in Table S2 2) detailing the differences in the reaction mechanisms, main reaction products, and influencing factors between the thermal and electrical decomposition of Silicone Rubber (SiR). S3 (gas products from thermal decomposition of SiR): infrared (IR) spectra (Fig. S1 3) of the gases released during the thermal decomposition of SiR at key characteristic temperatures (100 °C, 200 °C, 300 °C, 370 °C, 615 °C, and 754 °C) in both air and argon atmospheres. See DOI: https://doi.org/10.1039/d5ra07405c.

References

1 Z. Zhang, T. Liang, Z. Jiang, X. Jiang, J. Hu and G. Pang, *Polymers*, 2022, **14**, 4728.

2 R. Han, Y. Li, Q. Zhu and K. Niu, *Compos., Part C: Open Access*, 2022, **8**, 100249.
3 D. Gnanasekaran, *Power Res.*, 2025, **20**, 227–234.
4 Y. Zhu, Z. Qiu and R. Wu, *Case Stud. Therm. Eng.*, 2025, **73**, 106652.
5 R. Xia, B. Ouyang, Y. Wang, J. Yuan, K. Huang, C. Fang and Y. Wang, *Appl. Sci.*, 2023, **13**, 10406.
6 K. Komatsu, H. Liu, M. Shimada and Y. Mizuno, *Energies*, 2019, **12**, 2756.
7 J. Yu, Z. Zhang, W. Ren, D. Yang, D. Wu, Z. Ning, C. Fang and J. Wu, *Energies*, 2024, **17**, 708.
8 M. Akbari and A. A. Shayegani-Akmal, *Int. J. Electr. Power Energy Syst.*, 2023, **149**, 109049.
9 L. Long, L. Zeng, Y. Tian, W. Chen, J. Cheng, Z. Heng, Y. Chen, M. Liang, H. Zou, X. Liu and L. Yan, *Composites, Part A*, 2025, **198**, 109079.
10 J. Yang, Y. Xu, W. Jiang, B. Jiang and Y. Huang, *Ceram. Int.*, 2021, **47**, 21276–21284.
11 P. Rybiński, W. Żukowski and D. Bradło, *J. Therm. Anal. Calorim.*, 2015, **122**, 1307–1318.
12 M. Wu, T. Wu, Y. Luo, M. Xu, B. Niu, Y. Xing, Y. Zhang and D. Long, *J. Anal. Appl. Pyrolysis*, 2025, **188**, 107038.
13 K. Chenoweth, S. Cheung, A. C. T. van Duin, W. A. Goddard and E. M. Kober, *J. Am. Chem. Soc.*, 2005, **127**, 7192–7202.
14 J. Wang, G. Li, Z. Zhang, Q. Huang, B. Niu, Y. Zhang and D. Long, *Chem. Eng. J.*, 2024, **488**, 150728.
15 W. Yu, C. Liu, L. Tan, Q. Li, L. Xin and S. Wang, *Energy*, 2023, **284**, 129289.
16 J. Xiao, H. Zhang, X. Gao, H. Wang, G. Fang, B. Wang, C. Hong and S. Meng, *Chem. Eng. J.*, 2023, **458**, 141480.
17 O. Vryonis, T. Andritsch, A. S. Vaughan, P. Morshuis and A. Claverie, *J. Appl. Polym. Sci.*, 2025, **142**, e57358.
18 S. Mutha and A. Saratkar, Online Detection And Correction of Inter Turn Faults in Transformers, *2020 IEEE First International Conference on Smart Technologies for Power, Energy and Control (STPEC)*, 2020, pp. 1–5.
19 J. Song, Z. Huang, Y. Qin and X. Li, *Materials*, 2019, **12**, 1591.
20 Y. Liang, T. Gao, X. Wang, M. Sun and L. Gao, *Molecules*, 2018, **23**, 1861.
21 M. Tariq Nazir, B. T. Phung, M. Hoffman, S. Yu and S. Li, *Mater. Lett.*, 2017, **209**, 421–424.
22 Y. Zhang, W. Liu, Q. Zhou, Y. Meng, Y. Zhong, J. Xu, C. Xiao, G. Zhang and Y. Zhang, *Polymers*, 2023, **15**, 1224.
23 H. T. Truong, M. Hayashi, Y. Uesugi, Y. Tanaka and T. Ishijima, *Rev. Sci. Instrum.*, 2017, **88**, 065105.
24 X. Wei, C. Xu, Z. Jia and X. Wang, *J. Appl. Polym. Sci.*, 2021, **138**, 50203.
25 E. Kohls and M. Stein, *Contributions, Sec. Nat. Math. Biotech. Sci.*, 2017, **38**, 43.
26 L. Yu, S. Liu, B. Liu, Z. Mao, W. Huang, J. Peng and Y. Ao, *Nucl. Anal.*, 2022, **1**, 100005.
27 D. S. Tikhonov, I. Gordiy, D. A. Iakovlev, A. A. Gorislav, M. A. Kalinin, S. A. Nikolenko, K. M. Malaskeevich, K. Yureva, N. A. Matsokin and M. Schnell, *ChemPhysChem*, 2024, **25**, e202400547.
28 M. K. Kesharwani, B. Brauer and J. M. L. Martin, *J. Phys. Chem. A*, 2015, **119**, 1701–1714.
29 X. Li, Y. Zhang, L. Chen, X. Fu, J. Geng, Y. Liu, Y. Gong and S. Zhang, *Coatings*, 2023, **13**, 1668.
30 Z. Wang, X. Zhang, F. Wang, X. Lan and Y. Zhou, *SpringerPlus*, 2016, **5**, 790.
31 Y. Han, L. Zhang, B. Sun, L. Liu, G. Li, S. Li and Y. Wei, *High Voltage*, 2025, e70067.
32 A. Mihăilă, M. Macovei, L. Maieczki, M. Voduț, N. Tudorachi and G. Lisă, *Bul. Inst. Politeh. Iasi*, 2018, **64(68)**(1), 9–18.
33 A. Chaudhry and N. Billingham, *Polym. Degrad. Stab.*, 2001, **73**, 505–510.
34 A. Morawska-Chochół, M. Szumera, A. Młyniec and K. Pielichowska, *Materials*, 2024, **17**, 5608.
35 T. Radhakrishnan, *J. Appl. Polym. Sci.*, 1999, **73**, 441–450.
36 D. Allan, S. C. Radzinski, M. A. Tapsak and J. J. Liggat, *Silicon*, 2016, **8**, 553–562.
37 B. Tang, Q. Liang, L. Zhang, Z. Luo, C. Luo, M. Hu, J. Wang and L. Zhu, *J. Phys.: Conf. Ser.*, 2022, **2387**, 012032.
38 M. Alopaeus, GC-MS/SIM and HPLC method development for monitoring polydimethylsiloxane and its degradation products, Master's thesis, Åbo Akademi University, 2022.
39 P. Rybiński, W. Żukowski and D. Bradło, *J. Therm. Anal. Calorim.*, 2016, **125**, 1373–1386.
40 K. Lu and H. Chaney, *Materials*, 2025, **18**, 1412.